Identification of Novel Human HDAC8 Inhibitors by Pharmacophore-based Virtual Screening and Density Functional Theory Approaches

Seokmin Kim,[†,‖] Yuno Lee,[†,‖] Songmi Kim,[†,‖] Sang Jik Lee,[†] Phil Kyeong Heo,[†] Siu Kim,[†] Yong Jung Kwon,[‡] and Keun Woo Lee[†,*]

[†]*Division of Applied Life Science (BK21 Plus), Plant Molecular Biology and Biotechnology Research Center (PMBBRC), Research Institute of Natural Science(RINS), Gyeongsang National University (GNU), Jinju 52828, Republic of Korea. *E-mail: kwlee@gnu.ac.kr*

[‡]*Department of Chemical Engineering, Kangwon National University, Chunchon 200-701, Republic of Korea*

Received August 30, 2017, Accepted December 4, 2017, Published online January 17, 2018

Histone deacetylase (HDAC) enzyme plays a key role in deacetylation mechanism of N-terminal acetylated lysine residues in histone proteins. HDAC inhibitors have therapeutic potential as anticancer agents. A chemical feature-based pharmacophore model has been generated from known HDAC8 inhibitors (22 training set compounds) by a 3D QSAR pharmacophore generation approach. The top ranked hypothesis (Hypo1) contained three features of one hydrogen bond donor and two ring aromatics. Hypo1 was cross-validated using Fischer's randomization by shuffling the activity data in training set compounds. It was also validated by 248 test set compounds with a correlation coefficient of 0.851 between experimental and estimated activities. Thus, the validated Hypo1 was exploited for retrieving novel HDAC8 inhibitor candidates over 109,652 chemical compounds in both Maybridge and Chembridge chemical databases and then the screened compounds were tested by ADMET (absorption, distribution, metabolism, excretion, and toxicity) properties and Lipinski's rules to evaluate their druglikeness. Finally, 11 new lead candidates were obtained and the final three drug candidates from them were selected as potential inhibitors based on the results of molecular docking and density functional theory calculations.

Keywords: Histone deacetylase, Pharmacophore, Density function theory, Molecular docking, Virtual screening

Introduction

Histone deacetylase (HDAC) plays a key role in deacetylation mechanism of N-terminal acetylated lysine residues in histone proteins.[1–3] The deacetylation is one of the post-translational chromatin modifications that is controlled by HDACs and a family of functionally opposite histone acetyl transferase (HAT) enzymes.[4,5] This chromatin modification is required for preparing the chromatin accessible to a number of chromatin interacting proteins.[6] The HATs loosen the tight binding of histone and DNA by adding acetyl group to the N-terminal lysine residues in histone proteins and then it leads to the transcriptional activation.[7] This tight histone-DNA binding blocks the access of transcription factors and this is balanced by the HATs masking the positive charged lysine residues by adding acetyl groups.[8] In normal cells, the catalytic functions of these two enzymes, namely, HDAC and HAT, are well balanced, but in human cancer cells the interruption of this balance is frequently observed.[9–11] For these reasons, HDAC inhibitors can eliminate cancer cells, but normal cells have relatively more resistance to the inhibitor-induced cell death than cancer cells.[12,13]

Although HATs are present only in eukaryotic systems, the HDAC proteins are found in bacteria, fungi, plants, and animals.[14,15] These enzymes of HDAC are categorized into two major classes, zinc- and NAD-dependent HDACs. The HDAC enzymes are also divided into four classes, Classes I to IV based on their structures and domain organization. Whereas zinc-dependent HDAC enzymes belong to the Classes I, II, and IV, NAD-dependent ones are belonging to the Class III HDACs. The class I HDACs (HDACs 1–3 and 8) are homologous to the yeast Rpd3 deacetylase; class II HDACs (HDACs 4–7, 9, and 10) are related to the yeast Hda1 deacetylase; and class III proteins, sirtuins, are yeast Sir2 homologues. Class I and IV HDACs mainly expressed in the nucleus have a function as transcriptional co-repressors, which are related to cell proliferation and survival.[16] These HDAC enzymes are associated with a large widespread biological functions such as apoptosis, differentiation, proliferation, and senescence.[17] Because of these biological processes, development of an inhibitor for these enzymes will be helpful to cure a growing number of

‖These authors contributed equally to this work.

 © 2018 Korean Chemical Society, Seoul & Wiley-VCH Verlag GmbH & Co. KGaA, Weinheim

diseases including cancer, neurodegenerative, hereditary, and inflammatory diseases.[18–25]

HDAC inhibitors are structurally distinct comprised of three common structural characteristics: a metal-binding moiety (MBM), a hydrophobic spacer (HYS), and hydrophobic cap (HYC) group to bind with metal ion, binding tunnel residues, and active site entrance residues, respectively. Among the HDAC inhibitors, hydroxamic acid inhibitors including vorinostat (suberoylanilide hydroxamic acid, SAHA) approved by FDA are the most well studied group.[25] These derivatives of hydroxamic acid are highly selective to bind with HDAC8 showing 100 times greater than the other HDAC enzymes.[26]

From the many different HDAC enzymes, particularly HDAC8 expression correlates with the disease stage of neuroblastoma, a highly malignant pediatric tumor derived from precursor or immature cells of the sympathetic nervous system.[27,28] Except for HDAC8, functional HDACs are not found as catalytically active monomer form *in vitro* but as multiprotein complexes of higher molecular weight and also most of the purified HDAC enzymes are catalytically inactive.[29,30] In perspectives of a structural biology and drug discovery, HDAC8 is therefore considered as the best starting model than the other mammalian HDACs.

In this study, we focused on identifying novel potent inhibitor candidates through pharmacophore-based virtual screening and density functional theory (DFT) approaches. A 3D Quantitative Structure–activity Relationship (QSAR) pharmacophore model was generated for HDAC8 based on known HDAC8 inhibitors. The best and validated model was used as a 3D query for virtual screening of chemical databases to retrieve novel HDAC8 inhibitor candidates. The retrieved hit compounds were subsequently filtered by ADMET (absorption, distribution, metabolism, excretion, and toxicity) properties, Lipinski's rule of five, and molecular docking. Finally, the screened compounds were further evaluated by DFT calculating the orbital energy value and energy gap and molecular interactions obtained from molecular docking study. Thus, these results of this study can be utilized as a starting point in designing future HDAC8 inhibitors.

Methods

Selection of Data Sets, Training Set, and Test Set. All the pharmacophore modeling calculations were executed by Discovery Studio 3.5 (DS). The ligand-based pharmacophore modeling method, which is one of the most frequently used and powerful methods, can be divided into two different approaches for constructing pharmacophore model based on (1) common chemical feature of highly active compounds and (2) chemical structures and activity of training set compounds. To build the human HDAC8 data set, 270 compounds along with their inhibitory activity values (IC_{50}) were gathered from the same fluorescence assay collected using literature survey[31–45] and BindingDB web server.[46] The data set was divided into two different sets: training and test sets, which consist of 22 and 248 compounds, respectively. These 22 compounds were selected as training set to build 3D pharmacophore model based on structural diversity and IC_{50} values covering a wide activity range from 17 to 8104 nM (Figure 1). Both the training and test sets were categorized into three different groups based on their activities as highly active (≤100 nM, +++), moderate active (100–1000 nM, ++), and less active (> 1000 nM, +) compounds.

Pharmacophore Validation. The aim of validations of pharmacophore hypothesis is to evaluate whether the selected hypothesis is statistically significant to retrieve novel active compounds from a chemical database and to accurately predict their activity values. The best pharmacophore model was assessed by the cross-validation derived from Fischer's randomization method and test set validation to confirm its predictive ability.[47] Fischer's randomization run producing many various random spreadsheets with different significance levels (90, 95, and 99%) was performed by the 3D QSAR pharmacophore generation tool by scrambling the values of bioactivity in the training set. The significance level of the hypothesis was calculated based on the formula $S = 100 \times [1 - (1 + X)/Y]$, where S is a significance level; X represents the total number of hypotheses, which are having a total cost lower than the originally constructed hypothesis, and Y is the total number of initial HypoGen runs and random runs together. Here, we used $X = 0$ and $Y = (1 + 19)$, therefore 95% (= $100 \times [1 - (1 + 0)/20]$) significance level was selected. Test set compounds were used to validate whether the best pharmacophore model is able to estimate the activity values of diverse compounds as that of the active training set. The test set is consisted of 248 structurally diverse compounds with a wide range of experimental activity values. This test set validation was performed by ligand pharmacophore mapping tool implemented in DS.

Virtual Screening and ADMET Filtration. The validated pharmacophore model, Hypo1, was used as a 3D structural query for retrieving novel HDAC8 inhibitor candidates from two chemical databases namely Maybridge and Chembridge having a total number of 109 652 compounds. In order to filter out potential virtual lead compounds fitting well on the Hypo1, the pharmacophore-based database searching was performed by the ligand pharmacophore mapping tool with fast flexible search option. The number of retrieved hit compounds was further reduced by druglikeness properties such as ADMET properties[48,49] using ADMET descriptors tool and Lipinski's rule of five filtration in which compounds are considered to have bioavailability when the molecular weight is less than 500, an octanol–water partition coefficient (Log P) is not greater than 5, number of hydrogen bond donors (HBDs) is less than 5, and no more than 10 hydrogen bond acceptors using Filter by Lipinski rule tool[50] implemented in DS.

Molecular Docking. GOLD (Genetic Optimization for Ligand Docking) 5.2 program[51] was used to perform

 © 2018 Korean Chemical Society, Seoul & Wiley-VCH Verlag GmbH & Co. KGaA, Weinheim

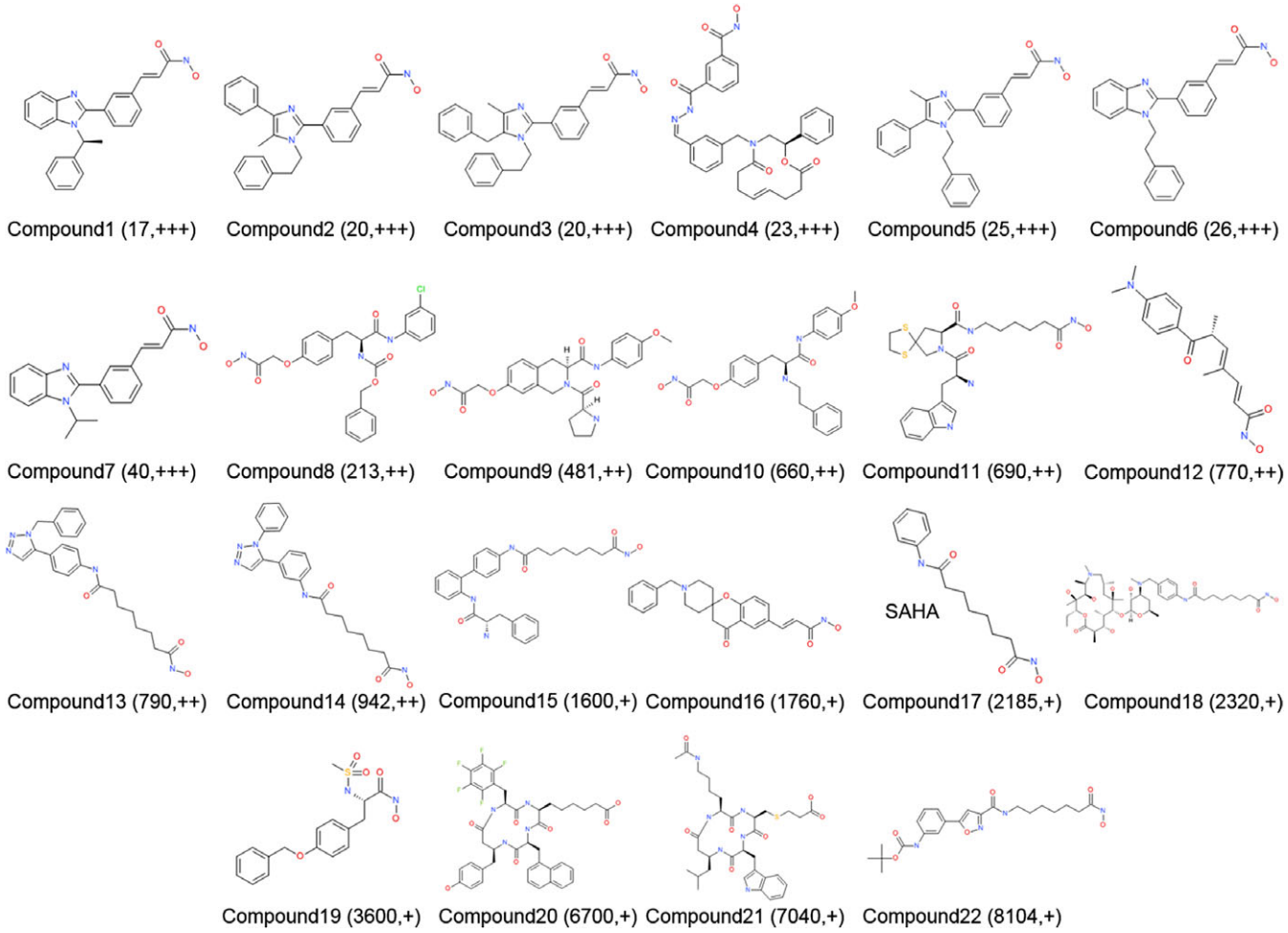

Figure 1. Chemical structures of 22 training set compounds along with their activity values. The IC_{50} value is indicated for each compound in nM. Categorized activity ranges represented as highly active (+++), moderate active (++), and less active (+).

molecular docking studies of the retrieved hit compounds into ligand binding site of HDAC8 enzyme. The GOLD program uses genetic algorithm approach for flexible docking of ligands into active site of the protein to explore the ensemble of ligand conformation with partial flexibility of the protein. The binding free energy ($\Delta G_{binding}$) of the hit compounds with protein was measured by ChemScore implemented in GOLD. The 3D crystal structure of HDAC8-inhibitor complex (PDB ID: 3SFF)[52] was obtained from Protein Data Bank (PDB, www.rcsb.org) and the co-crystalized inhibitor was used to define the active site for molecular docking studies. Among the co-crystalized structures, the lowest root mean square deviation (RMSD) value of 0.8 Å between docked pose and original conformation of crystal inhibitor was observed in the selected 3SFF structure. Unnecessary water molecules presented in the crystal structure were eliminated and protonation of the whole protein was performed with Clean Protein in DS. The ligand binding site for docking was defined as a sphere of radius 15 Å around the coordinates of the bound inhibitor. Molecular interactions were observed using analyze complex tool with 2D diagram as available in DS.

Density Functional Theory. DFT, which is the most successful and promising approach to compute the electronic properties of atoms, molecules, and solids,[53] was used to predict orbital energies of HDAC8 inhibitor candidates. The docking conformations of the 11 selected lead compounds from the molecular docking studies were subjected to the following DFT calculation as input ligands. From the results of molecular docking, favorable binding conformations of the compounds were obtained and thus it can be further used for computing the molecular orbital energies such as highest occupied molecular orbital (HOMO), lowest unoccupied molecular orbital (LUMO), and energy gap. The DMol^3 method implemented in DS was applied to calculate a variety of molecular and atomic properties with specific local Perdew-Wang (PWC) functional.[54] These electronic property calculations could be useful to select more reactive compounds.

Results and Discussion

In this study, ligand-based pharmacophore modeling methods were used to discover novel drug candidates for

 © 2018 Korean Chemical Society, Seoul & Wiley-VCH Verlag GmbH & Co. KGaA, Weinheim

Table 1. Results of top 10 pharmacophore hypotheses for statistical significance and predictive ability presented in cost values.

Hypo no.	Features	Total cost	RMSD	Correlation (*r*)
Hypo1	1 HBD, 2 RA	89.4219	0.535919	0.960851
Hypo2	1 HBD, 2 RA	90.1976	0.595997	0.951385
Hypo3	1 HBD, 2 RA	91.9395	0.719326	0.928231
Hypo4	1 HBD, 2 RA	92.5597	0.755598	0.920564
Hypo5	1 HBA, 2 RA	93.2672	0.786436	0.91391
Hypo6	1 HBD, 2 RA	95.3171	0.903876	0.884186
Hypo7	1 HBD, 2 RA, 1 Hy-Ali	95.4223	0.894415	0.887203
Hypo8	1 HBA, 2 RA	95.4346	0.89042	0.888392
Hypo9	1 HBD, 1 RA, 1 Hy-Ali	95.4717	0.902876	0.884744
Hypo10	1 HBD, 2 Hy-Ali	95.5822	0.912217	0.882062

treatment of cancer. Based on already known human HDAC8 inhibitors, the 3D pharmacophore models are constructed and the best model is selected depending on its predictive ability.

Hypothesis Generation. A set of 10 pharmacophore hypotheses was generated using 22 training set compounds (Figure 1). The statistical values such as RMSD and cost values for each hypothesis, and correlation coefficient (*r*) between experimental and predicted activity values of the inhibitors were calculated and listed in Table 1.

Among the 10 hypotheses, five hypotheses possess a common set of chemical features comprising one HBD and two ring aromatic (RA) groups (Figure 2). The top ranked pharmacophore hypothesis (Hypo 1) was characterized with the lowest total cost (89.422), the lowest RMSD (0.536), along with the highest correlation coefficient (0.961). Thus, the Hypo1 was considered as the most reasonable pharmacophore model for inhibiting the HDAC8 activity. To identify its predictive ability, the training set was classified into three different sets based on its activity values: highly active (≤100 nM, +++), moderate active (100–1000 nM, ++), and less active (> 1000 nM, +) (Table 2). In training set, Hypo1 overestimated two less active compounds as moderate active and underestimated the one moderate active compound as less active one. The predicted IC_{50} values for 19 of 22 training set compounds were within the same order of magnitude when compared with the experimental IC_{50} values. The compound 1, which is the most active molecule in the training set, was well fitted with all the chemical features in Hypo1 but the compound 22, which is the most inactive molecule, was failed to map with the HBD group (Figure 3). Hence, the HBD is one of essential factors to improve the potency of HDAC8 inhibitors.

Validation of Pharmacophore Hypothesis. Two statistical validation procedures such as Fischer's randomization and test set validations were conducted to evaluate whether the obtained pharmacophore hypothesis is able to select the active compounds.

Firstly, the cross-validation of Hypo1 was executed by Fischer's randomization to check its reliability. The method is performed by randomizing the activity data in training set compounds and then generating pharmacophore models based on the randomized set with exactly same conditions as used in original pharmacophore hypothesis generation. Totally, 19 random spreadsheets were generated to achieve 95% confidence level (significance = [1 − (1 + 0)/20] × 100% = 95%). The correlation coefficient values of 19 random pharmacophore spreadsheets were compared with those of the original hypothesis, Hypo1 showed that none of the 19 randomly generated spreadsheets are scored better than the Hypo1 (Figure 4). The 19 resulted random hypotheses showed a higher total cost, RMSD, and lower correlation coefficient values than the Hypo1 showing the superior quality of Hypo1.

Secondly, the statistical relevance of Hypo1 was validated by mapping of test set compounds with the best pharmacophore hypothesis, Hypo1, for predicting their estimated IC_{50} values. Totally, 248 test set compounds, which are distinct ones from training set compounds, were used in this validation. From the result of this approach, we have found that correlation coefficient value was 0.851, which shows strong correlation between experimental and estimated HDAC8 inhibitory activity values (Figure 5). Among 31 highly active compounds, only three compounds were underestimated as moderate active. Out of 117 moderate active compounds, only two compounds are overestimated as active and five compounds were predicted as less

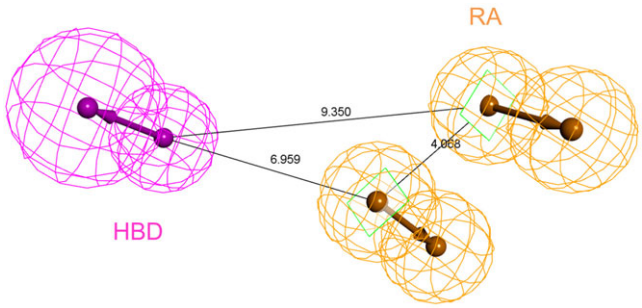

Figure 2. Three-dimensional representation of the top ranked hypothesis (Hypo1). RA and HDB features are represented in orange and magenta colors, respectively. All distances are in Å unit.

 © 2018 Korean Chemical Society, Seoul & Wiley-VCH Verlag GmbH & Co. KGaA, Weinheim

Table 2. Experimental inhibitory activity and the computed activity for the training set molecules based on the best pharmacophore model.

Compound	Experimental IC_{50} (nM)	Estimated IC_{50} (nM)	Error[a]	Activity scale[b]	Estimated activity scale[b]	Fit value[c]
1	17	21	1.2	+++	+++	5.28
2	20	18	−1.1	+++	+++	5.34
3	20	26	1.3	+++	+++	5.18
4	23	19	−1.2	+++	+++	5.32
5	25	21	−1.2	+++	+++	5.27
6	26	33	1.3	+++	+++	5.07
7	40	30	−1.3	+++	+++	5.12
8	213	820	3.9	++	++	3.68
9	481	720	1.5	++	++	3.73
10	660	760	1.1	++	++	3.72
11	690	1500	2.1	++	+	3.43
12	770	1000	1.3	++	++	3.59
13	790	1000	1.3	++	++	3.58
14	942	640	−1.5	++	++	3.79
15	1600	930	−1.7	+	++	3.62
16	1760	770	−2.3	+	++	3.71
17	2185	6500	3	+	+	2.78
18	2320	1800	−1.3	+	+	3.33
19	3600	2400	−1.5	+	+	3.21
20	6700	1700	−4	+	+	3.37
21	7040	6800	−1	+	+	2.76
22	8104	5300	−1.5	+	+	2.87

[a] The estimated IC_{50} is lower than the experimental IC_{50}; a value of 1 indicates that the estimated IC_{50} is equal to the experimental IC_{50}.
[b] Activity scale: +++, IC_{50} < 100 nM (highly active); ++, 1000 > IC_{50} ≥ 100 nM (moderate active); +, IC_{50} ≥ 1000 nM (inactive).
[c] Fit value denotes how well the features in the pharmacophore hypothesis overlap with the chemical features in the compound.

active compounds. All other test set compounds were predicted correctly or as better than their actual activities. Hence, this test set validation further confirms that the Hypo1 is able to discover novel drug candidates for HDAC8 inhibitor.

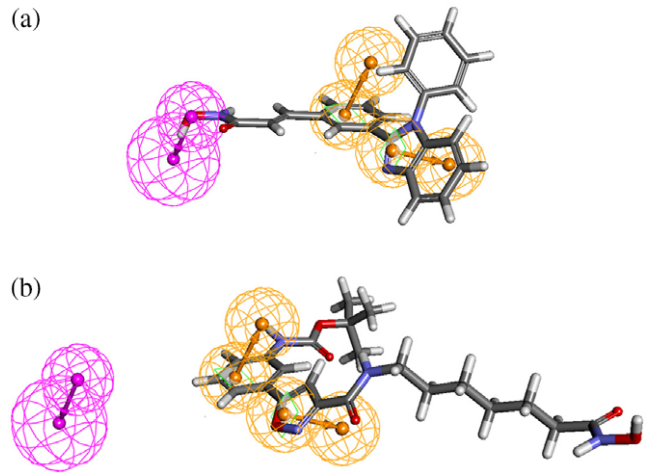

Figure 3. The aligned structures of the best pharmacophore model, Hypo1, with training set compounds 1 and 22. (a) Fitted conformation of the most active compound 1 in training set compounds with Hypo1. (b) Mapping of the least active compound 22 with Hypo1.

Virtual Screening and Druglikeness Prediction. The work procedure of virtual screening strategy carried out in the present study is shown in Figure 6. The validated pharmacophore hypothesis, Hypo1, was used as an input structural query for retrieving novel HDAC8 inhibitor candidates from Maybridge (59 652 compounds) and Chembridge (50 000 compounds) chemical databases. As a

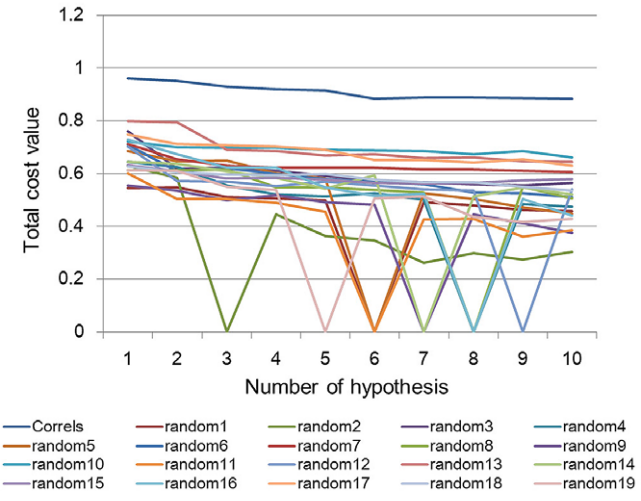

Figure 4. Results of Fischer's randomization showing the difference in total cost between 19 scrambled runs.

 © 2018 Korean Chemical Society, Seoul & Wiley-VCH Verlag GmbH & Co. KGaA, Weinheim

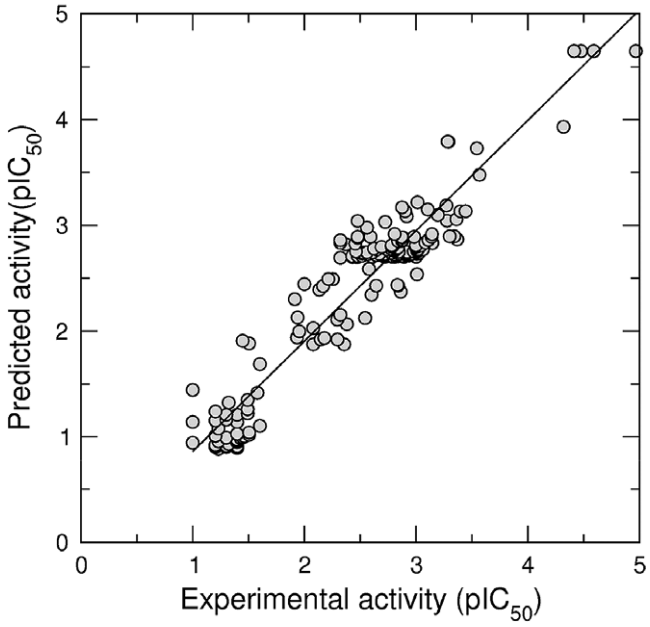

Figure 5. Plot of the correlation between experimental and predicted activity (pIC$_{50}$) by Hypo1 for the test set compounds. Correlation coefficient for test set compounds is 0.851.

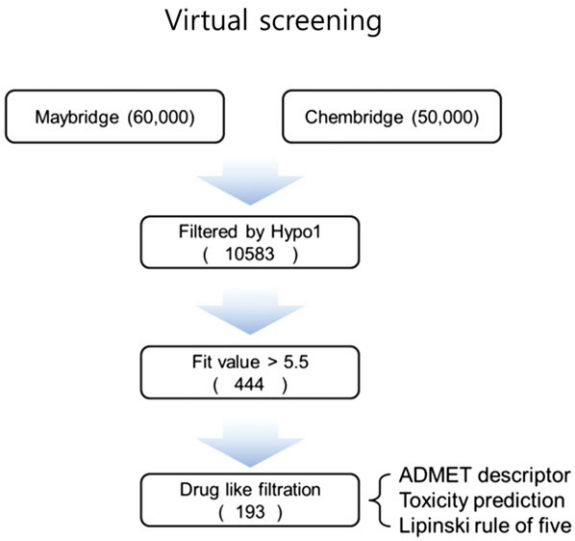

Figure 6. Flow chart of virtual screening procedure for novel HDAC8 inhibitor design.

result, a total of 10 583 hit compounds showed very well mapping with the Hypo1; among these, 444 were chosen for further analysis filtrated by maximum fit value of greater than 5.5 and satisfying all the chemical features of Hypo1. In order to select only the drug-like compounds, these hits were tested by ADMET and Lipinski's rule of five. ADMET properties such as solubility, hepatotoxicity, blood–brain barrier (BBB) penetration, cytochrome P450 (CYP) 2D6 inhibition, human intestinal absorption (HIA), and plasma protein binding (PPB) were computed with a broad range of ligand toxicity.

Subsequently, Lipinski's rule of five, which states that an octanol/water partition coefficient (Log$P$), molecular weight, HBDs, hydrogen bond acceptors, and rotatable bonds should be less than 5, 500, 5, 10, and 10, respectively, was applied to possess better druglikeness. A total of 193 hit compounds having favorable ADMET properties and within a Lipinski's rule of five were finally selected for further molecular docking study.

Final Hit Selection by Molecular Docking and DFT. To further refine the retrieved hit compounds, 193 hit compounds satisfying all druglikeness properties were docked into ligand binding site of HDAC8. The binding site was defined from the co-crystalized inhibitor in HDAC8 structure (PDB ID: 3SFF).[52] The obtained docking poses were ranked by estimated binding free energy, which is representing total free energy change that occurs on ligand binding. The 11 best hit compounds were selected by the binding free energy ($\Delta G_{\text{binding}}$), given by GOLD.

As an efficient filtration method after docking procedure, the orbital energies such as HOMO, LUMO, and energy gap(ΔE) values were also calculated for the 11 leads along with some training set compounds (Table 3). A smaller ΔE (between the LUMO and HOMO) of the lead compounds elucidates that the molecules are more reactive.[55] The wide value of ΔE in the leads is unfavorable for the electron to be excited from the HOMO to the LUMO, which subsequently leads to a weak-binding affinity. The atomic orbital composition of the molecular orbital for three hits, KM 05529, HTS10917, and SPB 02579, is shown in Figure 7. Among the 11 lead compounds, five lead compounds were selected based on their lowest ΔE values suggesting that the molecules would be reactive. Since these molecular electronic properties are responsible for the potent activity of HDAC8 inhibitors, it could be useful to determine whether the final lead compounds have the significant biological activity.

The binding poses of the five lead compounds at the active site of HDAC8 were analyzed based on molecular interactions with the key residues, Trp141, Asp178, His180, Asp267, and Tyr306, and catalytic Zn^{2+} ion for binding substrate, namely, acetylated lysine. The Zn^{2+} ion coordinated by Asp178, His180, and Asp267 is deeply buried in the narrow region in active site, located in between acetyl-lysine binding tunnel and acetate release channel.[52] The final three hit compounds were selected as the best potential inhibitors based on the number of critical interactions with the key residues and the metal ion. Binding poses of the final hit compounds at active site of HDAC8 are shown in Figure 8. The KM05529, HTS10917, and SPB02579 had a binding free energy of −51.564, −46.566, and −44.926 kJ/mol and the ΔE of 0.074, 0.101, and 0.101 eV, respectively. The KM05529 formed hydrogen bond interaction with catalytically important residues including His180, Asp267, and Gly304. Moreover, the π–π interaction was observed between Trp152 and aromatic ring of the KM05529 as depicted in Figure 9(a). The binding

 © 2018 Korean Chemical Society, Seoul & Wiley-VCH Verlag GmbH & Co. KGaA, Weinheim

Table 3. Molecular orbital energy value of hit leads and training set compounds.

Name	HOMO (eV)	LUMO (eV)	Δ*E* (LUMO–HOMO, eV)	IC_{50} (nM)
KM 05529	–0.174	–0.100	0.074	
KM 05992	–0.184	–0.093	0.091	
HTS 05992	–0.213	–0.117	0.096	
HTS 10917	–0.201	–0.100	0.101	
SPB 02579	–0.183	–0.082	0.101	
SEW 06390	–0.196	–0.093	0.103	
AW 01084	–0.186	–0.079	0.107	
KM 05945	–0.179	–0.067	0.112	
KM 05943	–0.183	–0.066	0.118	
HTS 01130	–0.182	–0.058	0.124	
KM 06090	–0.194	–0.068	0.127	
Training 1	–0.193	–0.093	0.099	17
Training 4	–0.188	–0.093	0.095	23
Training 5	–0.183	–0.088	0.095	25
Training 8	–0.194	–0.073	0.120	213
Training 11	–0.142	–0.018	0.124	690
Training 14	–0.187	–0.071	0.116	942
Training 17	–0.178	–0.028	0.150	2185
Training 19	–0.198	–0.056	0.142	3600

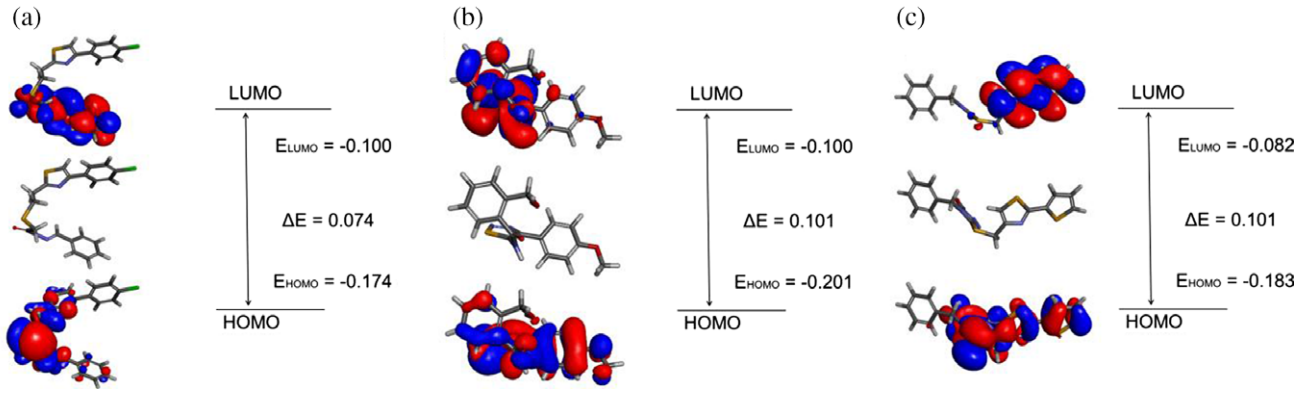

Figure 7. The orbital energy values and energy gap for final hit compounds: (a) KM05529, (b) HTS10917, and (c) SPB02579.

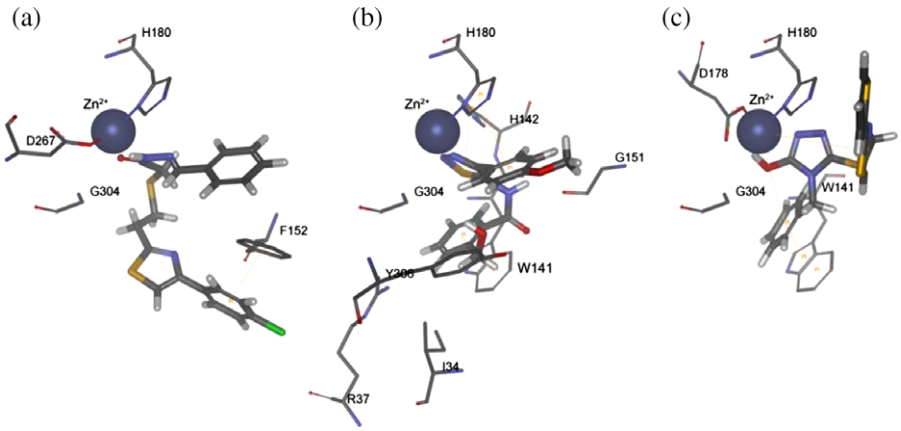

Figure 8. Docking modes of final hit compounds: (a) KM05529, (b) HTS10917, and (c) SPB02579. The final hit compound and interacting residue are represented as thick and thin stick models, respectively.

 © 2018 Korean Chemical Society, Seoul & Wiley-VCH Verlag GmbH & Co. KGaA, Weinheim

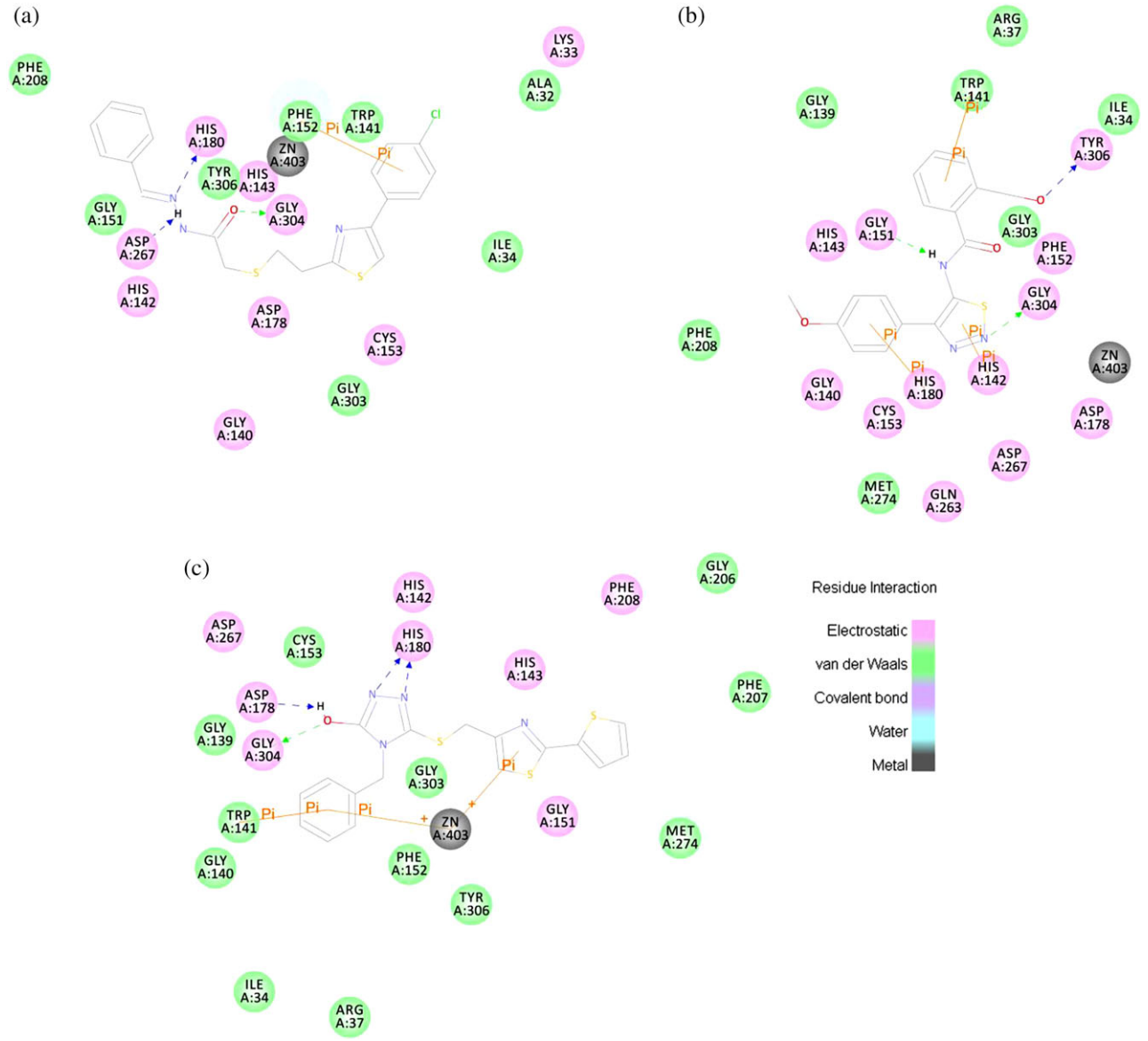

Figure 9. 2D diagram for interaction information of final hits: (a) KM05529, (b) HTS10917, and (c) SPB02579.

Table 4. Final hit compounds for HDAC8 inhibitor design.

	KM05529	HTS10917	SPB02579
Structure	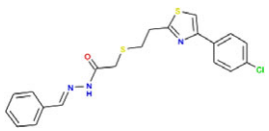	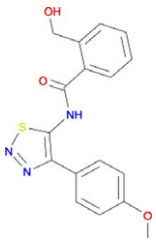	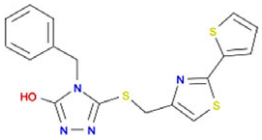
Estimated IC_{50}	8.401	8.795	9.379
Fit value	5.670	5.650	5.623
Goldscore fitness	85.026	78.557	83.656
Chemscore ΔG (kJ/mol)	−51.564	−46.566	−44.926
HOMO (eV)	−0.184	−0.201	−0.183
LUMO (eV)	−0.100	−0.100	−0.082
ΔE (eV)	0.074	0.101	0.101

 © 2018 Korean Chemical Society, Seoul & Wiley-VCH Verlag GmbH & Co. KGaA, Weinheim

mode of HTS10917 has shown that close contacts with Ile34 and Arg37, which are located in acetate release channel (Figure 9(b)). The binding conformation of SPB02579 has shown that two π–cation interactions with Zn^{2+} ion (Figure 9(c)), which is important catalytic metal ion for enzyme reaction.

From the results of molecular docking and DFT, we suggest that the three final hit compounds (Table 4) can have equivalent or greater binding affinity and molecular electronic properties compared with the most active compounds and thus the final hits could be used to design novel HDAC8 inhibitors.

Conclusion

In the present study, a statistically significant 3D pharmacophore model was generated based on a series of known HDAC8 inhibitors. The best pharmacophore model, Hypo1, consisting of one HBD and two RAs, was cross-validated by Fischer's randomization method with 95% statistical significance level as well as test set validation using 248 compounds. The test set showed a correlation coefficient of 0.851 between experimental and estimated IC_{50} values indicating satisfactory predictive ability. Based on the validated Hypo1, Maybridge and Chembridge databases were screened to find the diverse structures with novel scaffolds. The screened hit compounds were filtered by ADMET properties and Lipinski's rule of five to satisfy their druglikeness properties. A total of 193 compounds were docked into the active site of HDAC8 to further refine the hit compounds. The 11 lead compounds were selected based on the binding free energy ($\Delta G_{binding}$) obtained from the molecular docking study. The orbital energies such as HOMO, LUMO, and energy gap values were calculated to confirm the potencies of the lead compounds. Among the 11 lead compounds, five compounds were selected based on their lowest energy gap value, which is important for stability and energy transfer. Out of these, three final hits named KM05529, HTS10917, and SPB02579 were finally selected by considering their critical interactions with the key residues in HDAC8's active site. From these results, we suggest that final three hit compounds successfully mapped with all the pharmacophoric features of Hypo1 can be utilized in further designing of potent HDAC8 inhibitors.

Acknowledgments. This research was supported by Basic Science Research Program (2014R1A1A2059773) and Management of Climate Change Program (2010-0029084) through the National Research Foundation of Korea (NRF) funded by the Ministry of Education of Republic of Korea. And this work was also supported by the Next-Generation BioGreen 21 Program (PJ01106202) from Rural Development Administration (RDA) of Republic of Korea.

References

1. M. S. Finnin, J. R. Donigian, A. Cohen, V. M. Richon, R. A. Rifkind, P. A. Marks, R. Breslow, N. P. Pavletich, *Nature* **1999**, *401*, 188.
2. T. K. Nielsen, C. Hildmann, A. Dickmanns, A. Schwienhorst, R. Ficner, *J. Mol. Biol.* **2005**, *354*, 107.
3. S. M. Sternson, J. C. Wong, C. M. Grozinger, S. L. Schreiber, *Org. Lett.* **2001**, *3*, 4239.
4. A. Mai, S. Massa, R. Ragno, M. Esposito, G. Sbardella, G. Nocca, R. Scatena, F. Jesacher, P. Loidl, G. Brosch, *J. Med. Chem.* **2002**, *45*, 1778.
5. S. Vadivelan, B. Sinha, G. Rambabu, K. Boppana, S. A. Jagarlapudi, *J. Mol. Graphics Modell.* **2008**, *26*, 935.
6. T. Jenuwein, C. D. Allis, *Science* **2001**, *293*, 1074.
7. T. Sundarapandian, J. Shalini, S. Sugunadevi, L. K. Woo, *J. Mol. Graphics Modell.* **2010**, *29*, 382.
8. Y.-d. Chen, Y.-J. Jiang, J.-W. Zhou, Q.-S. Yu, Q.-D. You, *J. Mol. Graphics Modell.* **2008**, *26*, 1160.
9. Y. Chen, H. Li, W. Tang, C. Zhu, Y. Jiang, J. Zou, Q. Yu, Q. You, *Eur. J. Med. Chem.* **2009**, *44*, 2868.
10. O. H. Krämer, M. Göttlicher, T. Heinzel, *Trends Endocrinol. Metab.* **2001**, *12*, 294.
11. S. C. Lee, A. Bottaro, R. A. Insel, *Mol. Immunol.* **2003**, *39*, 923.
12. P. A. Marks, M. Dokmanovic, *Expert Opin. Investig. Drugs* **2005**, *14*, 1497.
13. G. Bi, G. Jiang, *Cell. Mol. Immunol.* **2006**, *3*, 285.
14. M. Paris, M. Porcelloni, M. Binaschi, D. Fattori, *J. Med. Chem.* **2008**, *51*, 1505.
15. L. J. Benson, J. A. Phillips, Y. Gu, M. R. Parthun, C. S. Hoffman, A. T. Annunziato, *J. Biol. Chem.* **2007**, *282*, 836.
16. I. Gregoretti, Y.-M. Lee, H. V. Goodson, *J. Mol. Biol.* **2004**, *338*, 17.
17. S. Thangapandian, S. John, S. Sakkiah, K. W. Lee, *Eur. J. Med. Chem.* **2010**, *45*, 4409.
18. M. Dokmanovic, P. A. Marks, *J. Cell. Biochem.* **2005**, *96*, 293.
19. E. Hahnen, J. Hauke, C. Tränkle, I. Y. Eyüpoglu, B. Wirth, I. Blümcke, *Expert Opin. Investig. Drugs* **2008**, *17*, 169.
20. B. Morrison, N. Majdzadeh, S. D'Mello, *Cell. Mol. Life Sci.* **2007**, *64*, 2258.
21. L. Brichta, Y. Hofmann, E. Hahnen, F. Siebzehnrubl, H. Raschke, I. Blumcke, I. Eyupoglu, B. Wirth, *Hum. Mol. Genet.* **2003**, *12*, 2481.
22. E. Hockly, V. M. Richon, B. Woodman, D. L. Smith, X. Zhou, E. Rosa, K. Sathasivam, S. Ghazi-Noori, A. Mahal, P. A. Lowden, *Proc. Natl. Acad. Sci. U.S.A.* **2003**, *100*, 2041.
23. I. Adcock, *Br. J. Pharmacol.* **2007**, *150*, 829.
24. D. Mottet, V. Castronovo, *Clin. Exp. Metastasis* **2008**, *25*, 183.
25. L. Pan, J. Lu, B. Huang, *Cell. Mol. Immunol.* **2007**, *4*, 337.
26. K. Krennhrubec, B. L. Marshall, M. Hedglin, E. Verdin, S. M. Ulrich, *Bioorg. Med. Chem. Lett.* **2007**, *17*, 2874.
27. G. M. Brodeur, *Nat. Rev. Cancer* **2003**, *3*, 203.
28. I. Oehme, H. E. Deubzer, D. Wegener, D. Pickert, J.-P. Linke, B. Hero, A. Kopp-Schneider, F. Westermann, S. M. Ulrich, A. von Deimling, *Clin. Cancer Res.* **2009**, *15*, 91.

 © 2018 Korean Chemical Society, Seoul & Wiley-VCH Verlag GmbH & Co. KGaA, Weinheim

29. J. E. Bolden, M. J. Peart, R. W. Johnstone, *Nat. Rev. Drug Discovery* **2006**, *5*, 769.
30. A. Vannini, C. Volpari, P. Gallinari, P. Jones, M. Mattu, A. Carfí, R. De Francesco, C. Steinkühler, S. Di Marco, *EMBO Rep.* **2007**, *8*, 879.
31. J. C. Bressi, R. d. Jong, Y. Wu, A. J. Jennings, J. W. Brown, S. O'Connell, L. W. Tari, R. J. Skene, P. Vu, M. Navre, *Bioorg. Med. Chem. Lett.* **2010**, *20*, 3138.
32. C. Wang, L. M. Henkes, L. B. Doughty, M. He, D. Wang, F.-J. Meyer-Almes, Y.-Q. Cheng, *J. Nat. Prod.* **2011**, *74*, 2031.
33. A. K. Oyelere, P. C. Chen, W. Guerrant, S. C. Mwakwari, R. Hood, Y. Zhang, Y. Fan, *J. Med. Chem.* **2008**, *52*, 456.
34. A. P. Kozikowski, S. Tapadar, D. N. Luchini, K. H. Kim, D. D. Billadeau, *J. Med. Chem.* **2008**, *51*, 4370.
35. Y. Chen, M. Lopez-Sanchez, D. N. Savoy, D. D. Billadeau, G. S. Dow, A. P. Kozikowski, *J. Med. Chem.* **2008**, *51*, 3437.
36. M. Varasi, F. Thaler, A. Abate, C. Bigogno, R. Boggio, G. Carenzi, T. Cataudella, R. Dal Zuffo, M. C. Fulco, M. G. Rozio, *J. Med. Chem.* **2011**, *54*, 3051.
37. R. Neelarapu, D. L. Holzle, S. Velaparthi, H. Bai, M. Brunsteiner, S. Y. Blond, P. A. Petukhov, *J. Med. Chem.* **2011**, *54*, 4350.
38. Y. Zhang, J. Feng, Y. Jia, X. Wang, L. Zhang, C. Liu, H. Fang, W. Xu, *J. Med. Chem.* **2011**, *54*, 2823.
39. A. P. Kozikowski, Y. Chen, A. Gaysin, B. Chen, M. A. D'Annibale, C. M. Suto, B. C. Langley, *J. Med. Chem.* **2007**, *50*, 3054.
40. Y. Zhang, J. Feng, Y. Jia, Y. Xu, C. Liu, H. Fang, W. Xu, *Eur. J. Med. Chem.* **2011**, *46*, 5387.
41. W. Tang, T. Luo, E. F. Greenberg, J. E. Bradner, S. L. Schreiber, *Bioorganic Med. Chem. Lett.* **2011**, *21*, 2601.
42. J. C. Canzoneri, P. C. Chen, A. K. Oyelere, *Bioorg. Med. Chem. Lett.* **2009**, *19*, 6588.
43. D. V. Smil, S. Manku, Y. A. Chantigny, S. Leit, A. Wahhab, T. P. Yan, M. Fournel, C. Maroun, Z. Li, A.-M. Lemieux, *Bioorg. Med. Chem. Lett* **2009**, *19*, 688.
44. X.-C. Cheng, R.-L. Wang, Z.-K. Dong, J. Li, Y.-Y. Li, R.-R. Li, *Bioorg. Med. Chem.* **2012**, *20*, 5738.
45. Y. Zhang, J. Feng, C. Liu, H. Fang, W. Xu, *Bioorg. Med. Chem.* **2011**, *19*, 4437.
46. T. Liu, Y. Lin, X. Wen, R. N. Jorissen, M. K. Gilson, *Nucleic Acids Res.* **2007**, *35*, D198.
47. Y. Lee, N. Bharatham, K. Bharatham, K. W. Lee, *Bull. Korean Chem. Soc.* **2007**, *28*, 561.
48. W. J. Egan, K. M. Merz, J. J. Baldwin, *J. Med. Chem.* **2000**, *43*, 3867.
49. W. J. Egan, G. Lauri, *Adv. Drug Delivery Rev.* **2002**, *54*, 273.
50. C. A. Lipinski, F. Lombardo, B. W. Dominy, P. J. Feeney, *Adv. Drug Delivery Rev.* **2012**, *64*, 4.
51. G. Jones, P. Willett, R. C. Glen, A. R. Leach, R. Taylor, *J. Mol. Biol.* **1997**, *267*, 727.
52. L. Whitehead, M. R. Dobler, B. Radetich, Y. Zhu, P. W. Atadja, T. Claiborne, J. E. Grob, A. McRiner, M. R. Pancost, A. Patnaik, *Bioorg. Med. Chem.* **2011**, *19*, 4626.
53. L. J. Bartolotti, K. Flurchick, *Rev. Comput. Chem.* **1996**, *7*, 187.
54. J. P. Perdew, Y. Wang, *Phys. Rev. B* **1992**, *45*, 13244.
55. A. N. Queiroz, B. A. Gomes, W. M. Moraes Jr., R. S. Borges, *Eur. J. Med.* **2009**, *44*, 1644.

 © 2018 Korean Chemical Society, Seoul & Wiley-VCH Verlag GmbH & Co. KGaA, Weinheim